ATMOSPHERIC ENVIRONMENT: X 18 (2023) 100217

Contents lists available at ScienceDirect

Atmospheric Environment: X

journal homepage: www.journals.elsevier.com/atmospheric-environment-x

Improving the comparability of FFF-3D printing emission data by adjustment of the set extruder temperature

Chi-Long Tang *, Stefan Seeger, Mathias Röllig

Federal Institute for Materials Research and Testing (BAM), Unter den Eichen 87, 12205, Berlin, Germany

ARTICLE INFO

Keywords:
FFF-3D printer
Ultrafine particles
Infrared thermography
Thermocouple
Emission test chamber
Indoor air quality

ABSTRACT

Fused filament fabrication (FFF) is a material extrusion-based technique often used in desktop 3D printers. Polymeric filaments are melted and are extruded through a heated nozzle to form a 3D object in layers. The extruder temperature is therefore a key parameter for a successful print job but also one of the main emission driving factors as harmful pollutants (e.g., ultrafine particles) are formed by thermal polymer degradation. The awareness of potential health risks has increased the number of emission studies in the past years. However, studies usually refer their calculated emission data to the printer set extruder temperature for comparison purposes. In this study, we used a thermocouple and an infrared camera to measure the actual extruder temperature and found significant temperature deviations to the displayed set temperature among printer models. Our result shows that printing the same filament feedstocks with three different printer models and with identical printer set temperature resulted in a variation in particle emission of around two orders of magnitude. A temperature adjustment has reduced the variation to approx. one order of magnitude. Thus, it is necessary to refer the measured emission data to the actual extruder temperature as it poses a more accurate comparison parameter for evaluation of the indoor air quality in user scenarios or for health risk assessments.

1. Introduction

Fused filament fabrication (FFF) is a well-established additive manufacturing technique often applied in small-scale desktop 3D printers. Since the last decade, 3D printing has attained more and more popularity among hobbyist and semi-professionals for the use as home fabrication devices, for educational purposes or for rapid prototyping in small and medium-sized enterprises. In FFF, a thermoplastic filament is extruded through a heated nozzle head in order to build a 3D object layer by layer on a printing bed. In practice, the extrusion temperature is above the melting point or the glass transition temperature for crystalline or amorphous polymers, respectively. Thus, thermal degradation and formation of ultrafine particles (UFP; particle diameter of 100 nm or less) occur which are generally released indoors during a 3D printing process (Stephens et al., 2013; Kim et al., 2015; Deng et al., 2016; Yi et al., 2016; Azimi et al., 2016; McDonnell et al., 2016; Steinle, 2016; Mendes et al., 2017; Floyd et al., 2017; Kwon et al., 2017; Stabile et al., 2017; Vance et al., 2017; Zhang et al., 2017; Seeger et al., 2018; Gu et al., 2019; Poikkimäki et al., 2019; Beisser et al., 2020; Jeon et al., 2020; Katz et al., 2020; Secondo et al., 2020; Dunn et al., 2020; Sittichompoo et al., 2020; Alberts et al., 2021; Viitanen et al., 2021; Dobrzyńska et al., 2021; Chýlek et al., 2021; Bernatikova et al., 2021; Stefaniak et al., 2021; Manoj et al., 2021; Tang and Seeger, 2022; Romanowski et al., 2022; Saliakas et al., 2022). These findings raised the awareness, as UFP exposure has been reported to increase the risk of adverse health effects (Oberdörster et al., 1995, 2004, 2005; Hong and Jee, 2020; Schraufnagel, 2020). Since the pioneer emission study of Stephens et al. (2013) this research topic has been largely expanded. However, an objective comparison of emission data within previous studies seems difficult due to the multiplicity of different scientific approaches including varying measurement setups, diverse filament materials and printer brands, variation in printer settings and printed objects, and different calculation basis of assessment parameters. Hence, a basis for comparison can only be created by a systematic characterization of emission influencing factors in conjunction with filament materials and printer hardware. To determine the filament-specific emission, we proposed a standard test method which puts emphasis on filament materials and minimizes bias from printer hardware and settings (Tang and Seeger, 2022). The printer hardware related emission, however, is more challenging to characterize because of the numerous

* Corresponding author.
E-mail address: chi-long.tang@bam.de (C.-L. Tang).

https://doi.org/10.1016/j.aeaoa.2023.100217
Received 13 February 2023; Received in revised form 18 March 2023; Accepted 25 March 2023
Available online 27 March 2023

existing hardware designs and setting options. Azimi et al. (2016) and Zhang et al. (2017) had already pointed out that the emission is influenced by the printer brand. Studies have shown that overheating of the feedstock is one of the main emission factors as degradation of thermoplastics is temperature driven. Increasing the extruder temperature for a given filament generally enhances the particle emission as stated in many studies (Azimi et al., 2016; Deng et al., 2016; Mendes et al., 2017; Kwon et al., 2017; Stabile et al., 2017; Zhang et al., 2017; Seeger et al., 2018; Gu et al., 2019; Jeon et al., 2020; Poikkimäki et al., 2019; Tang and Seeger, 2022). Our previously published results suggest that even a temperature increase by only 5 °C elevates the particle emission level (Tang and Seeger, 2022), hence the temperature setting is a crucial parameter for the investigation and intercomparison of emission data. We like to point out here that overheating can occur if the user intendedly choses the wrong setting or unintendedly due to a systematic deviation between setting and actual extruder temperature.

The extruder temperature (also referred to as nozzle temperature in some studies) is set by the printer's control hardware or software. It is normally measured by a built-in temperature sensor which is positioned next to a heating cartridge and inserted in a heating block. The nozzle is bolted on the bottom of the heating block (see Fig. S1 in Supplementary data). So, strictly speaking, the sensor measures the temperature of the heating block and not the actual extruder temperature. The heat transfer to the nozzle depends on the thermal conductivity and specific heat capacity of the heating block and nozzle material. Offsets and temporal deviations between set extruder temperature and actual extruder temperature are possible. These depend on the printer's temperature control and the measurement uncertainty of the built-in sensor. We expect that across the market of commercial low- and mid-price FFF-3D printer substantial systematic deviations between set temperatures and actual extruder temperatures will occur. This may systematically bias the comparison of results from previous emission studies, e.g., 50 FFF-3D printing publications were discussed in the review article from Romanowski et al. (2022), as these generally refer to the set temperatures rather than to the actual extruder temperatures at which a filament material is operated. In addition, an incorrect temperature setting may lead to exceeding the manufacturer temperature recommendation for a filament and hence could influence the derived health risks for users. Despite the fact that extrusion temperature is in the literature often regarded as a main emission driver, we are not aware of any study focusing on the above-mentioned problem. This motivated us to measure actual extruder temperatures at different low- and high temperature settings for a selection of printers and materials. For temperature measurements we chose infrared thermography (Dinwiddie et al., 2014; Seppala and Migler, 2016) which recorded the spatial and temporal temperature profiles through thermal imaging and thermocouple sensor which recorded the temporal temperature profiles at nozzles during operation. We examined different influencing factors, e.g., filament type, nozzle, and heating block material, which may affect the temporal and spatial temperature distribution.

This investigation aims to present a robust method for measuring the actual extruder temperature. This helps users to avoid overheating the feedstock and may enable unbiased comparison of emissions from different printer models and feedstocks in indoor air quality and health risk assessments.

2. Materials and methods

2.1. Printers and filaments

Three FFF-3D printers with different technical features were used. The Craftbot 2 (abbr. CB2, Craftbot Ltd, Hungary) was already used in our previous study (Tang and Seeger, 2022). Its cover hood with a built-in HEPA filter was removed during emission testing. A MK8 brass nozzle (M6 threading size, 5 mm threading length) with an output diameter of 0.4 mm was applied. The operating temperature range is 180–260 °C and 50–110 °C for extruder and printing bed, respectively.

The Creatbot F160 Peek (abbr. CP, Henan Creatbot Technology Limited, PRC) utilizes two different hotends for specific temperature ranges. The low temperature hotend (aluminum heating block) and a MK8 brass nozzle (abbr. CP(L-B)) is sufficient for the standard temperature range between 180 and 260 °C. The printer is originally designed for printing industrial polymers such as PEEK, PEKK or PEI at higher temperatures of up to 420 °C. In this case, the high temperature hotend (brass heating block) in combination with MK8 hardened steel nozzles (abbr. CP(H–S)) are installed. The printer is fully enclosed in a housing, consisting of a metal frame and polycarbonate panes. The printing bed can be heat up to 150 °C and a built-in heater maintains the interior housing temperature at a maximum of 70 °C. For emission testing, the housing lid was dismounted, and the interior heater was turned off.

The Anycubic i3 Mega S (abbr. AnyM, Shenzhen Anycubic Technology Co., Limited, PRC) operates within the standard temperature ranges of 180–260 °C for the extruder and up to 110 °C for the printing bed. This printer utilizes E3D V6 brass nozzles (M6 threading size, 7.5 mm threading length, smaller nozzle head than MK8). AnyM is not equipped with an enclosure which impedes the heating up of the printing bed inside the testing chamber under active air circulation. Due to this fact, we decided to limit the maximum printing bed temperature to 80 °C during emission testing. The emission from the printing bed is expected to be negligible (Tang and Seeger, 2022).

While the particle emission from extrusion of a polymeric filament material is expected to be the dominant contribution, the printer hardware also contributes. Due to different technical features of the tested printers, we expected hardware emissions at different levels. This so-called printer blank is unavoidable due to release of particles from heated components (e.g., hotend, printing bed) but should ideally be negligible or at least constant at a low level in order to make a printer suitable as a reference printer for filament emission tests. To investigate this, the printer emissions from AnyM, CB2 and CP(L-B) were measured at their respective maximum testing temperatures without inserting a filament (in Section 3.4).

All printers are compatible with 1.75 mm diameter filaments. Three common polymers ABS, PLA and PETG and a copper-filled PLA were chosen to examine the extruder temperature during operation (Table 1, measurement T). Based on the experiences from our last emission study (Tang and Seeger, 2022), four filaments - two PLA and two ABS products which cover three orders of magnitude in total number of emitted particles TP (TP: 10^9-10^{11}) with good repeatability - were selected for emission testing (Table 1, measurement E).

2.2. Strand printing method (SPM)

SPM was applied in this study as a standard printing procedure. In

Table 1
Selection of filaments (TP data reference from Tang and Seeger (2022)). E: Emission and T: Temperature.

Filament	Product	Measurements	TP_{Mean} [-]	RSD [%]
BIO-S-02	Extrudr, GreenTEC Black (PLA)	E	$2.8{\cdot}10^9$	3.7
PLA-P-B-01	filamentworld, PLA PLUS Blau (Blue)	E	$1.3{\cdot}10^{10}$	8.4
ABS-T-01	filamentworld, ABS Glasklar (Transparent)	E	$4.1{\cdot}10^9$	21.4
ABS-W-01	filamentworld, ABS Schneeweiß (White)	E/T	$3.2{\cdot}10^{11}$	16.0
PLA-W-01	filamentworld, PLA Schneeweiß (White)	T	–	–
PETG-S-01	filamentworld, PETG Schwarz (Black)	T	–	–
MF–CO–03	ColorFabb, CopperFill (PLA)	T	–	–

SPM, the filament is extruded at a constant rate over time for a defined volume or length and is deposited on the printing bed without printing a 3D object. A detailed description can be found in Tang and Seeger (2022). Individual SPM G codes, i.e., standardized printer commands, were developed for each printer model because of technical differences in hardware and software (see examples in Supplementary data Figs. S2–4). The comparability was ensured as the total extruded filament length remains at 800 mm with a maximum deviation of 5% for every printer model and filament combination (see Fig. S5 in Supplementary data).

2.3. Temperature measurements

Two different methods were applied to determine the extruder temperature. A thermocouple (BB ML NL500 1.0, NiCr–Ni type K, B + B Thermo-Technik GmbH, Germany) with a diameter of 1 mm was directly inserted into the nozzle with good thermal contact to the inner nozzle surface. It measures the temperature very close to the nozzle outlet, representing approximately the actual polymer temperature when exiting the nozzle (see Fig. S1). The sensor's temperature range is between −200 °C and 1100 °C at an uncertainty of ±1.5 K or ±0.004*T in accordance with DIN EN 60584 class 1. The thermocouple was connected via an Almemo® connector (ZA 9020 FS) to an Almemo® 2590 data logger (Ahlborn Mess-und Regelungstechnik GmbH, Germany). The data recording frequency was 0.5 Hz. While the thermocouple enabled temperature measurements in the empty nozzle only, surface temperature measurements of the heated empty nozzle as well as of the filled nozzle during extrusion of a filament could be made additionally by means of infrared thermography. The thermograms allow time dependent temperature point evaluations as well as the evaluation of temperature line profiles on the nozzle surface.

An infrared camera (VarioCam HR, InfraTec GmbH Infrarotsensorik und Messtechnik, Germany) with a 30 mm lens and an additional close-up lens was used for thermal imaging. The camera covers a spectral range from 8 to 14 μm and has calibrated temperature ranges for −40 to +120 °C, 0 to +300 °C and +100 to +600 °C. The optical resolution is 640 x 480 pixel, and the noise equivalent temperature difference (NETD) is 30 mK at 30 °C. The measurement uncertainty is ±1.5 K or ±0.015*T for temperature above 100 °C. For a better temperature measurement precision, the nozzle surface was coated with paint (Tetenal Camera Paint Spray Black deep-matt, Tetenal 1847 GmbH, Germany) in order to achieve a defined emissivity of 0.93 ± 0.02 (see Fig. S6 in Supplementary data). The camera was positioned as close to the nozzle as possible in order to monitor the heating up to the set temperature (see Fig. S7). The printing bed was kept unheated. All measurements were carried out in a climatic room (T = 23 °C ± 2 K, RH = 42% ± 7%). The data were recorded at 2 Hz and were evaluated with the thermographic software IRBIS Professional 3.1.80.

2.4. Emission test chamber

The printers were tested inside a 1-m^3 emission test chamber which complies with the standard ISO 16000-9:2006 and the basic criteria of the DE-UZ-219 guideline (Blauer Engel, 2021). The climate condition maintains at T = 23 °C ± 2 K and RH = 50% ± 5%. Filtered and particle free clean air is supplied at an exchange rate of 1 h^{-1}. The chamber operates with a slight overpressure to prevent contamination from outside. Particle measuring instruments were positioned next to the chamber and aerosol sampling tubes were connected via ducts.

2.5. Particle measurement and data evaluation

A condensation particle counter (CPC, model 3775, TSI Inc., USA) measured the total particle number concentration (TPNC) in the size range from 4 to 3000 nm. The lower particle concentration limit (LLOD) is approximately 0.1 cm^{-3}. Prior to each measurement, a background TPNC of less than 100 cm^{-3} in the chamber was ensured by clean air ventilation. Particle number size distributions (PNSD) were scanned by an aerosol spectrometer (EEPS™, model 3090, TSI Inc., USA) in the size range of 5.6–560 nm. Additionally, an optical particle size spectrometer (OPSS, model 1.108, GRIMM Aerosol Technik Pouch GmbH, Germany) monitored a possible contribution from the size range between 0.3 and 20 μm to the TPNC, which was in all measurements negligible and hence not considered for further evaluation. EEPS™ and CPC recorded the TPNC at 1 Hz and the OPSS operated at 1/6 Hz.

From the CPC data the evaluation parameter TP (Total number of emitted particles) was calculated in accordance with DE-UZ-219 and as outlined briefly below. TP represents the time integral of the particle emission rate during a print job with consideration of particle losses in the chamber because of air exchange, wall adhesion and other loss mechanisms. It can be assumed in accordance with previous results that during the short period of strand extrusion (approx. 12 min) no relevant agglomeration and coagulation of particles occur (Tang and Seeger, 2022). Therefore, the particle loss is depicted in a simplified manner by the decrease in TPNC after the stop of printer activities, i.e., stop of emissions. The particle loss constant β is defined in equation (1), where C_1 and C_2 are the corresponding TPNCs at times t_1 and t_2, respectively, taken after the emission has stopped, i.e., after stop of printing.

$$\beta = \frac{\ln\left(c_1/c_2\right)}{t_2 - t_1} \tag{1}$$

The parameter TP is calculated according to equation (2):

$$TP = V_C\left(\frac{\Delta C_P}{t_{stop} - t_{start}} + \beta \bullet C_{AV}\right)\left(t_{stop} - t_{start}\right) \tag{2}$$

With the chamber volume V_C and $t_{stop} - t_{start}$ marking the period between start of heating up and the end of printing. ΔC_P is the difference in TPNC and C_{AV} is the arithmetic mean of TPNC between t_{stop} and t_{start}.

3. Results and discussions

3.1. Temperature measurement of empty nozzles by thermocouple and infrared camera

At the respective printer set temperatures the nozzle temperatures were measured by the thermocouple and by the infrared camera as described above. In Fig. 1, thermograms of the four empty printer-hotend combinations in steady state after heating up to the same set temperature of 230 °C are shown. The yellow lines, labelled as "L3″, represent the surface temperature line profiles. Significant temperature differences between the tested printers and deviations to the set temperature could be observed. The temperature line profiles (L3) are compared in Fig. 2. All nozzles revealed a surface temperature decrease between inlet and outlet of approximately 10 K. The subsequent sharp temperature drops mark the end of the nozzle tips. One printer (AnyM) shows an actual nozzle temperature above the set temperature, for the other printers the set temperature overestimates the actual nozzle temperature. (For a correct interpretation of Figs. 1 and 2 it has to be noted that the length of the AnyM nozzle is shorter than that of the other nozzles: AnyM: 5 mm; CB2: 8 mm; CP(L-B) and CP(H–S): 8 mm, see Fig. S6). The points labelled as "P2" in the thermograms in Fig. 1 indicate the positions at which the nozzles surface temperatures close to the measuring point of the thermocouple are evaluated.

3.2. Measurement of systematic deviations between set temperature and nozzle temperature

The set extruder temperatures for the three printers were increased stepwise within the individual operating ranges from 180 to 260 °C and for the CP(H–S) from 180 to 420 °C in 10 K increments (see Fig. 3). The temperatures of the empty nozzles were measured by a) the

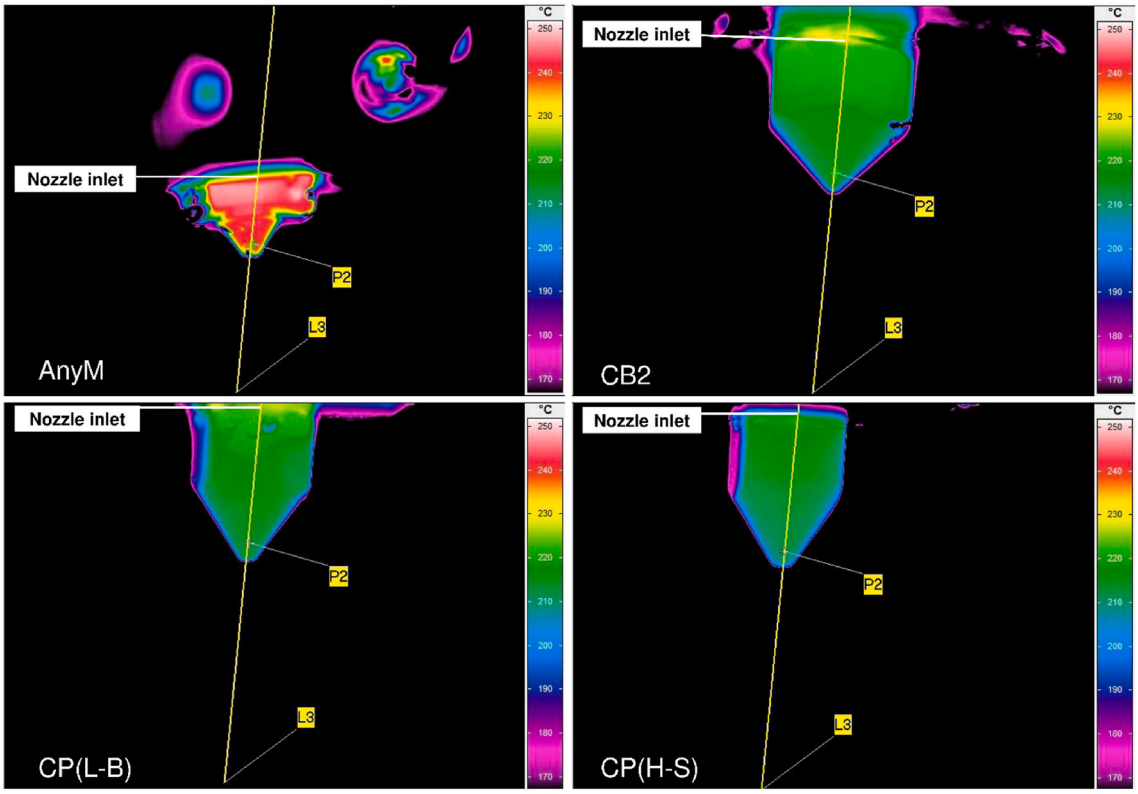

Fig. 1. Steady state thermograms of empty nozzles with printer's set temperature at 230 °C. Locations of temperature point measurements (P2), temperature line profiles (L3, yellow lines) and the nozzle inlet are marked. Note: The nozzle length of the AnyM printer is shorter than that of the other printers. (For interpretation of the references to color in this figure legend, the reader is referred to the Web version of this article.)

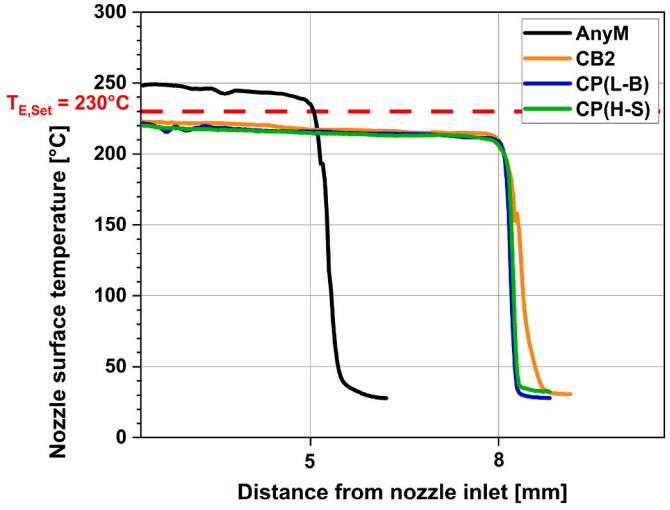

Fig. 2. Nozzle surface temperature line profiles (yellow lines (L3) shown in Fig. 1) for the investigated printers at set extruder temperature $T_{E,Set}$ = 230 °C (red dotted line). Printer CP was measured with two different hotend and nozzle types. (Note: The AnyM nozzle length is 5 mm only.). (For interpretation of the references to color in this figure legend, the reader is referred to the Web version of this article.)

thermocouple in the nozzle and b) by infrared thermography at the P2 position, as described above. Typical PID (proportional–integral–derivative) temperature control patterns were recorded for all tested printers. After an overshoot, the amplitudes show a damped oscillation until converging to the set point. CP has two hotend combinations as recommended by the manufacturer: a low temperature hotend with brass nozzle (L-B) and a high temperature hotend with hardened steel nozzle (H–S). Interestingly, CB2 and AnyM showed superior PID control compared to CP(L-B) when using brass nozzles as temperatures converge and reach a steady level in less than 60 s. CP(L-B), on the other hand, initially seems to have a suboptimal control setting as the temperature oscillates with approx. 2.5 K maximum amplitudes. However, the oscillation is noticeably lower when the high temperature hotend with hardened steel nozzle was used instead. Fig. S8 in the Supplementary data indicates that the hotend material has a greater influence on the PID performance than the nozzle material showing a convergence to set point at a quicker pace. It should be noted that the heating block of the high temperature hotend is made of brass whereas the low temperature heating block is made of aluminum. In general, aluminum has larger thermal diffusivity compared to brass, resulting in faster thermal heat uptake and transfer. The PID controller was probably primarily programmed for a brass hotend, since the printer's standard setting is for PEEK which normally requires a temperature above 380 °C.

The temperatures over time from the thermocouple and the infrared camera corresponded well for AnyM but indicate constantly lower IR temperatures of approximately 6 K for CB2 and 3 K for CP(L-B). On the one hand, this is within the measurement uncertainty of both instruments (e.g., at 260 °C the expanded measurement uncertainty is U = 6.05 K for infrared camera and U = 1.20 K for thermocouple with a coverage factor of k = 2; see Supplementary data). On the other hand, we suggest that the difference in nozzle head geometry (AnyM: length = 5 mm, width = 7 mm; CB2: length = 8 mm, width = 8 mm; CP: length = 8 mm, width = 6 mm; see Fig. S6 in Supplementary data) is responsible for this discrepancy. Larger surface area and wall thickness may increase the cooling effect by convective heat loss on the outer nozzle surface, hence resulting in lower temperatures as seen by the infrared camera. The same was observed for CP(H–S) heated up to approx. 290 °C. Above,

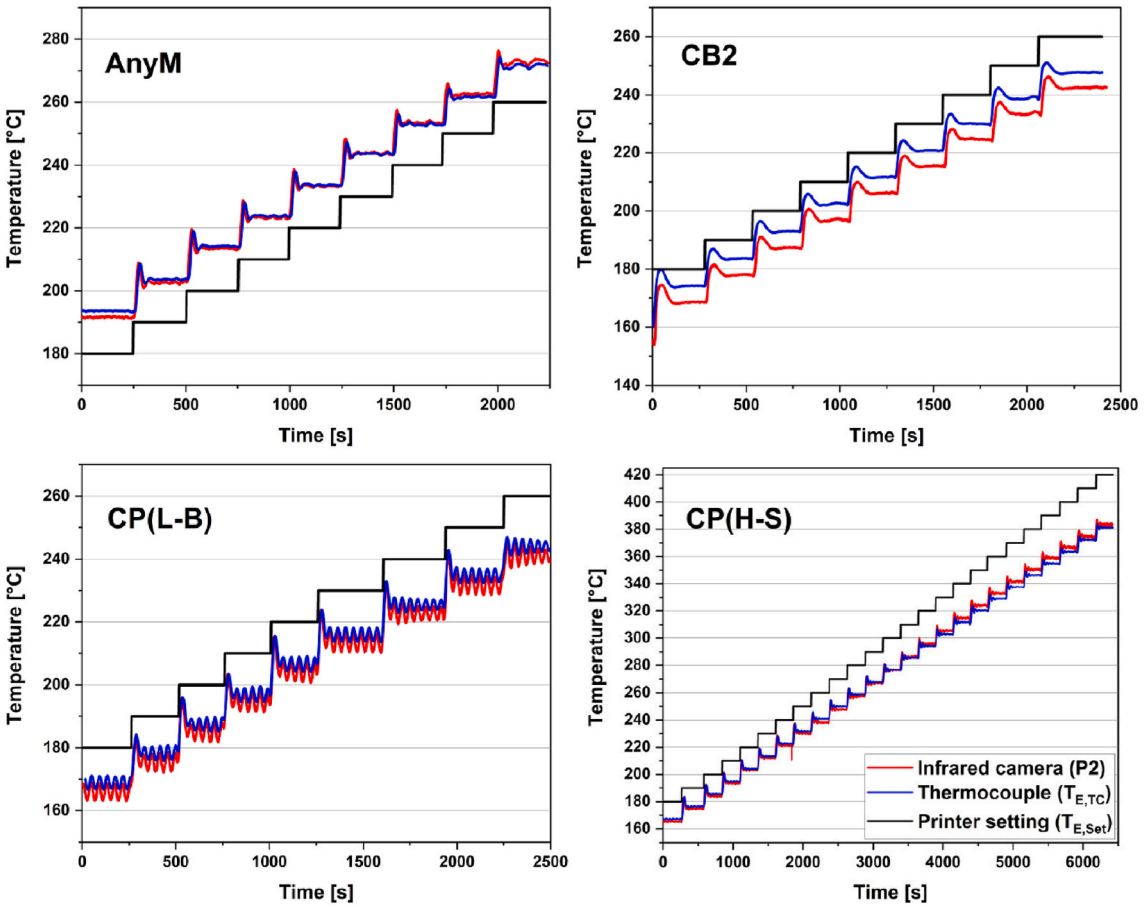

Fig. 3. Set temperature variation for all tested printers including two hotend/nozzle combinations for CP.

the infrared camera values exceeded the thermocouple temperatures. This could be a result from the camera calibrations in the two used operating ranges (0–300 °C and 100–600 °C).

For all three printers, the temperature measurements consistently revealed a substantial deviation from the printer's set temperature. Taking the thermocouple as the reference, the actual extruder temperatures of CB2 were in average 6 K–12 K below the set value. ΔT slightly increases with the set temperature. The same was observed for CP(L-B), the actual extruder temperatures were in average 11 K–16 K below the set temperature. AnyM, on the other hand, has actual extruder temperatures well above the set values, the ΔT average was about 11 K–14 K and did not increase with the set temperature. For a typical printer setting at 230 °C for example, the printer AnyM has an actual extruder temperature of 244 °C while CB2 has 221 °C and CP(L-B) has 216 °C.

It can be concluded from our findings, that great care must be taken in comparing emission results even when the same filament is operated on different printer hardware and with the same set temperature. Even in this case, the actual nozzle temperatures may differ and hence influence the resulting emission levels to a large extend. This will be discussed in the next section. Moreover, the quality of a printed object is also influenced by an accurate setting of the extruder temperature. Our results indicate that printing an object on two printers at the same settings, namely the same set temperature, but with different ΔT between set temperature and nozzle temperature may result in different object quality.

To examine a real printing scenario, the extruder temperature was measured with the infrared camera during strand extrusion using printer CB2. This printer reveals extruder temperatures below the set temperature. During extrusion of all tested filaments only minor temperature increase was measured at P2 (PLA-W-01: 3 K, PETG-S-01: 2 K, MF–CO–03: 3 K, ABS-W-01: 4 K) (see Fig. S9). This increase may be a result of the heat transfer from the molten filament material to the nozzle outlet (see Fig. S10). It can be concluded that also in the case of filament extrusion the temperature deviation between printer setting and nozzle is existent.

3.3. Extrusion temperature adjustment

It can be assumed that for a given filament, operated at different printers, the particle emission levels will be much closer together if the actual extruder temperatures were the same. Hence, for emission testing, we consider the determination of offsets between set temperatures and extruder temperatures as a necessary step in order to adjust all printers under test to the same extrusion temperatures. Adjusted extruder temperature settings can be calculated using the data from Fig. 3 in the previous section. A linear correlation between set temperatures and actual extruder temperatures was established for each printer within its temperature operating range. For this purpose, the arithmetic means of the temperature plateaus, measured by the thermocouple were calculated for each temperature step and plotted against the set temperature as depicted in Fig. 4. The thermocouple was considered as the reference sensor for several reasons: Firstly, it has a considerably lower measurement uncertainty compared to IR thermography. Secondly, it is not influenced by ambient conditions, i.e., cooling by ventilated air. Thirdly, the set-up, the measurement, and the data evaluation seem to be manageable as part of a measuring standard for a test laboratory. On the other hand, the pivotal advantage of thermal imaging is the real time measurement of the spatial nozzle temperature distribution during operation. While this technique seems a bit too elaborate to derive correction factors, we could at least verify that the extruder temperature

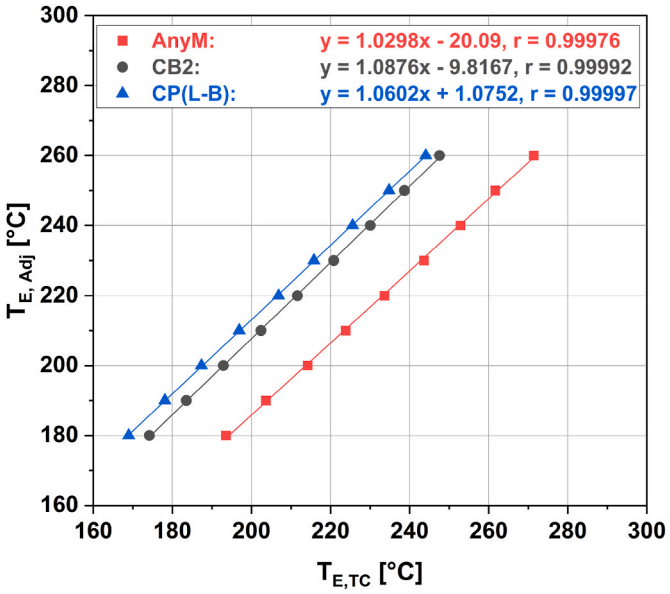

Fig. 4. Temperature adjustment for CB2, AnyM and CP(L-B). Each data point represents arithmetic means at steady-state temperature levels. $T_{E,TC}$ depicts the reference temperature measured by the thermocouple and $T_{E,Adj}$ is the extruder temperature for adjustment.

is only marginally affected by filament extrusion. Further studies should however complement the presented findings. Adjusted extruder set temperatures ($T_{E,Adj}$) can be calculated for each printer using the regression functions displayed in Fig. 4. For example, the temperature setting of AnyM should be only 217 °C in order to set the extruder to actual 230 °C while the same extruder temperature is achieved for the CB2 if its adjusted set temperature is 240 °C. The adjusted printer-specific temperatures for the tested filaments are listed in Table 2. It should be noted that the printers only allow temperature settings rounded to a whole number. For this study, only the CP(L-B) design of the CP printer was adjusted as this combination is recommended for the standard printing range of up to 260 °C, i.e., the same operating range as for CB2 and AnyM.

3.4. Printer hardware emission

Different heights of printer blanks may occur due to printer-specific features, such as e. g. heating block coating, which are heat-exposed. Such coatings are often made of plastic to stabilize the temperature for better printing results and to avoid deposition of filament residues on the heating block. The silicon coating of AnyM is directly heat-exposed and emitted a substantial number of particles during the printer blank test. Removing the coating reduced the TPNC by 99% to a concentration level below LLOQ (Lower Limit of Quantification) (see Figs. S11 and S12 in Supplementary data). The LLOQ for the calculation of TP is approx. 1000 cm^{-3} which equals at an air exchange of 1 per hour in a 1 m^3 chamber a TP value of about 10^9 particles. The coating of CB2 is not removeable but the printer showed an acceptable level of TP = $6.8{\cdot}10^9$, i.e., below 10% of the total emission of ABS-T-01 at 240 °C. The aluminum hotend of CP is not equipped with any coating and showed a printer blank close to the LLOQ. The measured printer blanks are available in the Supplementary data in Figs. S13 and S14.

To quantify any effect of coating removal from the AnyM, its extruder temperatures with and without coating were compared within the operating temperature range with a thermocouple and no differences were observed. Hence, the AnyM was used without coating for comparative emission measurements.

3.5. Filament emission

The emission parameter TP was determined from the CPC data for each combination of filament and printer with the uncorrected set temperature ($T_{E,Set}$) and secondly with the adjusted set temperature ($T_{E,Adj}$). The results are described in Table 2 in detail and are illustrated in Fig. 5. Fig. 5 highlights two aspects: a) the reproducibility of the particle emission from each printer and filament, and b) the scatter of emission data from different printers before and after set temperature adjustment.

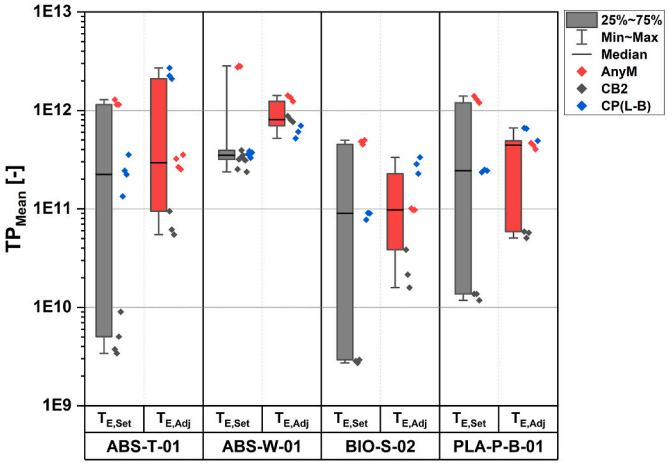

Fig. 5. TP values illustrated as color-coded squares for respective printer. The boxplots show the TP scatter ranges before and after temperature adjustment. $T_{E,Set}$: original printer set temperature, $T_{E,Adj}$: adjusted extruder temperature. (For interpretation of the references to color in this figure legend, the reader is referred to the Web version of this article.)

Table 2
Average TP (TP_{Mean}) and geometric mean diameter (GMD) of the particle number size distribution at the end of the printing process with the corresponding relative standard deviation in parentheses. The printer original set temperatures ($T_{E,Set}$) and the adjusted extruder temperatures ($T_{E,Adj}$) are listed. TP_{Mean} and GMD marked with an asterisk include measurements from Tang and Seeger (2022).

Filament	Printer	$T_{E,Set}$ [°C]	N	TP_{Mean} [-]	GMD [nm]	$T_{E,Adj}$ [°C]	N	TP_{Mean} [-]	GMD [nm]
ABS-W-01	CB2	230	8	$3.13{\cdot}10^{11}$* (16.0%)	56.6* (5.3%)	240	3	$8.14{\cdot}10^{11}$* (7.1%)	52.9* (3.1%)
ABS-W-01	AnyM	230	3	$2.79{\cdot}10^{12}$ (1.4%)	50.7 (1.6%)	217	3	$1.34{\cdot}10^{12}$ (6.8%)	48.8 (1.6%)
ABS-W-01	CP(L-B)	230	4	$3.62{\cdot}10^{11}$ (6.7%)	45.7 (2.3%)	245	3	$6.07{\cdot}10^{11}$ (14.7%)	51.2 (3.8%)
ABS-T-01	CB2	230	4	$5.30{\cdot}10^{9}$* (48.6%)	N/A*	240	3	$7.03{\cdot}10^{10}$ (30.3%)	27.1 (12.9%)
ABS-T-01	AnyM	230	3	$1.20{\cdot}10^{12}$ (6.8%)	19.7 (2.7%)	217	4	$2.98{\cdot}10^{11}$ (16.0%)	17.9 (5.0%)
ABS-T-01	CP(L-B)	230	4	$2.39{\cdot}10^{11}$ (37.9%)	16.7 (4.3%)	245	3	$2.35{\cdot}10^{12}$ (13.3%)	23.0 (3.5%)
PLA-P-B-01	CB2	210	3	$1.31{\cdot}10^{10}$* (8.4%)	N/A*	219	3	$5.55{\cdot}10^{10}$ (7.8%)	58.2 (3.1%)
PLA-P-B-01	AnyM	210	3	$1.30{\cdot}10^{12}$ (7.7%)	38.7 (1.6%)	196	3	$4.37{\cdot}10^{11}$ (7.2%)	37.9 (2.0%)
PLA-P-B-01	CP(L-B)	210	3	$2.43{\cdot}10^{11}$ (2.9%)	27.7 (2.0%)	224	3	$6.01{\cdot}10^{11}$ (16.1%)	30.5 (1.5%)
BIO-S-02	CB2	210	3	$2.83{\cdot}10^{9}$* (3.7%)	N/A*	219	3	$2.53{\cdot}10^{10}$ (46.5%)	66.2 (8.3%)
BIO-S-02	AnyM	210	3	$4.77{\cdot}10^{11}$ (5.0%)	55.2 (1.5%)	196	3	$9.87{\cdot}10^{10}$ (2.0%)	58.4 (1.7%)
BIO-S-02	CP(L-B)	210	3	$8.61{\cdot}10^{10}$ (8.7%)	37.8 (3.5%)	224	3	$2.81{\cdot}10^{11}$ (18.9%)	41.6 (1.5%)

For each combination of printer and filament the TP values from repeated measurements (color-coded data points in Fig. 5) are closely together and thus indicating good reproducibility in accordance with the typical SPM measurement uncertainties reported in Tang and Seeger (2022) for the printer model CB2. This result shows promising good reproducibility of emission tests with SPM for two more commercial FFF-3D printer models.

The scatter of the TP values is for each investigated filament depicted in Fig. 5 as box plots. Grey boxes indicate the scatter in TP without set temperature adjustment while the red boxes reveal the effect of adjustment. Without adjustment the scatter range covers between 2 and 2.5 orders of magnitude for three out of four filaments and only one order of magnitude for the ABS-W-01 filament. With set temperature adjustment (red boxes) the scatter ranges are substantially reduced to 1.5 orders of magnitude for ABS-T-01 and much less for the other materials. The effect is strongest for the ABS-W-01 filament: Here, the large scatter range is driven by the fact that TP values from CB2 and CP(L-B) are closely together and are much lower than the TP values from the AnyM. This discrepancy is after temperature adjustment drastically reduced and the resulting scatter range is much less than one order of magnitude. Thus, emission data from different printers without temperature adjustment lack comparability due to divergent extruder temperatures. A much better comparability of the emission data from three printers processing four filament materials could be achieved after adjusting the extruder temperatures as described.

The remaining discrepancies between emission data from different printers may be attributed to their individual heating process and temperature control. The particle number size distributions (PNSD) indicate that particle formation during the filament extrusion still varies between printers kept at same extruder temperature. In all cases, CB2 had emitted the largest particle sizes followed by AnyM and CP(L-B) which is quite consistent with the determined TP. Examples are shown in Figs. S15 and S16, when printing with CB2 the PNSD of PLA-P-B-01 was clearly shifted towards bigger particles (GMD around 58 nm) compared to 38 nm for AnyM and 31 nm for CP(L-B). Similar PNSDs were observed for the filament BIO-S-02 between CB2 and CP(L-B) data. ABS-W-01 and ABS-T-01, on the other hand, showed similar PNSDs for all three printers (see Figs. S17 and S18).

4. Conclusion

Our result shows that printing identical filament feedstocks on three different printer models with same set temperature resulted in a variation in particle emission of around two orders of magnitude. Temperature adjustments, ensuring the same actual extruder temperature on all printers, reduced the variation to approx. one order of magnitude, i.e., after temperature adjustment, the printer hardware effect on the emissions could be reduced significantly. This is an important advantage for future FFF-3D printer emission studies as the impact of systematic discrepancies of temperatures can be avoided and an objectifiable basis for data comparison can be achieved. Our findings also suggest that the user should set the extruder temperature with caution as some commercial FFF printers may have a higher actual extruder temperature than displayed. Unintended overheating not only affects the print quality but may cause unnecessarily increased exposure to particle emissions.

Funding sources

This work was funded by the German Environment Agency (UBA) under the grant FKZ 3721 62 2010.

CRediT authorship contribution statement

Chi-Long Tang: Conceptualization, Data curation, Formal analysis, Investigation, Methodology, Project administration, Software, Validation, Visualization, Writing – original draft, Writing – review & editing. **Stefan Seeger:** Conceptualization, Funding acquisition, Methodology, Project administration, Resources, Software, Supervision, Writing – original draft, Writing – review & editing. **Mathias Röllig:** Data curation, Formal analysis, Investigation, Methodology, Software, Validation, Writing – review & editing.

Declaration of competing interest

The authors declare that they have no known competing financial interests or personal relationships that could have appeared to influence the work reported in this paper.

Data availability

Data will be made available on request.

Acknowledgement

The authors thank Prof. Dr. Andreas Held, Technical University of Berlin, and Dr. Mathias Ziegler, BAM, for a review of the manuscript prior to submission to the journal.

Appendix A. Supplementary data

Supplementary data to this article can be found online at https://doi.org/10.1016/j.aeaoa.2023.100217.

References

Alberts, E., Ballentine, M., Barnes, E., Kennedy, A., 2021. 'Impact of metal additives on particle emission profiles from a fused filament fabrication 3D printer'. Atmos. Environ. 244, 117956.

Azimi, P., Zhao, D., Pouzet, C., Crain, N.E., Stephens, B., 2016. 'Emissions of ultrafine particles and volatile organic compounds from commercially available desktop three-dimensional printers with multiple filaments'. Environ. Sci. Technol. 50, 1260–1268.

Beisser, R., Werner, S., Heinrich, B., Pelzer, J., 2020. 'Emissions from desktop 3D printers-more closely examined-Part 1'. Gefahrst. Reinhalt. Luft 80, 53–60.

Bernatikova, S., Dudacek, A., Prichystalova, R., Klecka, V., Kocurkova, L., 2021. 'Characterization of ultrafine particles and VOCs emitted from a 3D printer'. Int. J. Environ. Res. Publ. Health 18, 929.

Blauer Engel (Blue Angel) The german ecolabel, 2021. 'Environmentally friendly printers and multifunction devices (DE-UZ 219)'. https://www.blauer-engel.de/en/productworld/printers-and-multifunction-devices/laser-led-devices-toner. (Accessed 14 December 2022).

Chýlek, R., Kudela, L., Pospíšil, J., Šnajdárek, L., 2021. 'Parameters influencing the emission of ultrafine particles during 3D printing'. Int. J. Environ. Res. Publ. Health 18, 11670.

Deng, Y., Cao, S.-J., Chen, A., Guo, Y., 2016. 'The impact of manufacturing parameters on submicron particle emissions from a desktop 3D printer in the perspective of emission reduction'. Build. Environ. 104, 311–319.

Dinwiddie, R., Kunc, V., Lindal, J., Post, B., Smith, R., Love, L., Duty, C., 2014. 'Infrared imaging of the polymer 3D-printing process'. Thermosense: thermal infrared applications XXXVI, 9105.

Dobrzyńska, E., Kondej, D., Kowalska, J., Szewczyńska, M., 2021. 'State of the art in additive manufacturing and its possible chemical and particle hazards-review'. Indoor Air 31, 1733–1758.

Dunn, K.L., Hammond, D., Menchaca, K., Roth, G., Dunn, K.H., 2020. 'Reducing ultrafine particulate emission from multiple 3D printers in an office environment using a prototype engineering control'. J. Nanoparticle Res. 22, 112.

Floyd, E.L., Wang, J., Regens, J.L., 2017. 'Fume emissions from a low-cost 3-D printer with various filaments'. J. Occup. Environ. Hyg. 14, 523–533.

Gu, J., Wensing, M., Uhde, E., Salthammer, T., 2019. 'Characterization of particulate and gaseous pollutants emitted during operation of a desktop 3D printer'. Environ. Int. 123, 476–485.

Hong, G., Jee, Y.-K., 2020. 'Special issue on ultrafine particles: where are they from and how do they affect us?'. Exp. Mol. Med. 52, 309–310.

ISO, 2006. Indoor Air - Part 9: Determination of the Emission of Volatile Organic Compounds from Building Products and Furnishing - Emission Test Chamber Method. Beuth, Berlin. ISO 16000-9:2006).

Jeon, H., Park, J., Kim, S., Park, K., Yoon, C., 2020. 'Effect of nozzle temperature on the emission rate of ultrafine particles during 3D printing'. Indoor Air 30, 306–314.

Katz, E.F., Goetz, J.D., Wang, C., Hart, J.L., Terranova, B., Taheri, M.L., Waring, M.S., DeCarlo, P.F., 2020. 'Chemical and physical characterization of 3D printer aerosol emissions with and without a filter attachment'. Environ. Sci. Technol. 54, 947–954.

Kim, Y., Yoon, C., Ham, S., Park, J., Kim, S., Kwon, O., Tsai, P.-J., 2015. 'Emissions of nanoparticles and gaseous material from 3D printer operation'. Environ. Sci. Technol. 49, 12044–12053.
Kwon, O., Yoon, C., Ham, S., Park, J., Lee, J., Yoo, D., Kim, Y., 2017. 'Characterization and control of nanoparticle emission during 3D printing'. Environ. Sci. Technol. 51, 10357–10368.
Manoj, A., Bhuyan, M., Banik, S.R., Ravi Sankar, M., 2021. 'Review on particle emissions during fused deposition modeling of acrylonitrile butadiene styrene and polylactic acid polymers'. Mater. Today Proc. 44, 1375–1383.
McDonnell, B., Guzman, X.J., Doblack, M., Simpson, T.W., Cimbala, J.M., 2016. 3D printing in the wild: a preliminary, investigation of air quality in college maker spaces. In: Proceedings of the 27th Annual International Solid Freeform Fabrication Symposium 2016. Austin, Texas, USA.
Mendes, L., Kangas, A., Kukko, K., Mølgaard, B., Säämänen, A., Kanerva, T., Flores Ituarte, I., Huhtiniemi, M., Stockmann-Juvala, H., Partanen, J., Hämeri, K., Eleftheriadis, K., Viitanen, A.K., 2017. 'Characterization of emissions from a desktop 3D printer'. J. Ind. Ecol. 21, S94–S106.
Oberdörster, G., Celein, R.M., Ferin, J., Weiss, B., 1995. Association of particulate air pollution and acute mortality: involvement of ultrafine particles? Inhal. Toxicol. 7, 111–124.
Oberdörster, G., Oberdörster, E., Oberdörster, J., 2005. 'Nanotoxicology: an emerging discipline evolving from studies of ultrafine particles'. Environ. Health Perspect. 113, 823–839.
Oberdörster, G., Sharp, Z., Atudorei, V., Elder, A., Gelein, R., Kreyling, W., Cox, C., 2004. 'Translocation of inhaled ultrafine particles to the brain'. Inhal. Toxicol. 16, 437–445.
Poikkimäki, M., Koljonen, V., Leskinen, N., Närhi, M., Kangasniemi, O., Kausiala, O., Dal Maso, M., 2019. 'Nanocluster aerosol emissions of a 3D printer'. Environ. Sci. Technol. 53, 13618–13628.
Romanowski, H., Bierkandt, F.S., Luch, A., Laux, P., 2022. 'Summary and derived Risk Assessment of 3D printing emission studies'. Atmos. Environ. 294, 119501.
Saliakas, S., Karayannis, P., Kokkinopoulos, I., Damilos, S., Gkartzou, E., Zouboulis, P., Karatza, A., Koumoulos, E.P., 2022. 'Fused filament fabrication 3D printing: quantification of exposure to airborne particles'. J. Compos. Sci. 6, 119.
Schraufnagel, D.E., 2020. 'The health effects of ultrafine particles'. Exp. Mol. Med. 52, 311–317.
Secondo, L.E., Adawi, H.I., Cuddehe, J., Hopson, K., Schumacher, A., Mendoza, L., Cartin, C., Lewinski, N.A., 2020. Comparative analysis of ventilation efficiency on ultrafine particle removal in university MakerSpaces. Atmos. Environ. 224, 117321.
Seeger, S., Brödner, D., Jacobi, T., Rasch, F., Rothhardt, M., Wilke, O., 2018. 'Emissions of fine and ultrafine particles and volatile organic compounds from different filament materials operated on a low-cost 3D printer'. Gefahrst. Reinhalt. Luft 78, 79–87.
Seppala, J.E., Migler, K.D., 2016. 'Infrared thermography of welding zones produced by polymer extrusion additive manufacturing'. Addit. Manuf. 12, 71–76.
Sittichompoo, S., Kanagalingam, S., Thomas-Seale, L.E.J., Tsolakis, A., Herreros, J.M., 2020. 'Characterization of particle emission from thermoplastic additive manufacturing'. Atmos. Environ. 239, 117765.
Stabile, L., Scungio, M., Buonanno, G., Arpino, F., Ficco, G., 2017. 'Airborne particle emission of a commercial 3D printer: the effect of filament material and printing temperature'. Indoor Air 27, 398–408.
Stefaniak, A.B., Bowers, L.N., Cottrell, G., Erdem, E., Knepp, A.K., Martin, S., Pretty, J., Duling, M.G., Arnold, E.D., Wilson, Z., Krider, B., LeBouf, R.F., Virji, M.A., Sirinterlikci, A., 2021. 'Use of 3-dimensional printers in educational settings: the need for awareness of the effects of printer temperature and filament type on contaminant releases'. ACS Chem. Health & Saf. 28, 444–456.
Steinle, P., 2016. 'Characterization of emissions from a desktop 3D printer and indoor air measurements in office settings'. J. Occup. Environ. Hyg. 13, 121–132.
Stephens, B., Azimi, P., El Orch, Z., Ramos, T., 2013. 'Ultrafine particle emissions from desktop 3D printers'. Atmos. Environ. 79, 334–339.
Tang, C.-L., Seeger, S., 2022. 'Systematic ranking of filaments regarding their particulate emissions during fused filament fabrication 3D printing by means of a proposed standard test method'. Indoor Air 32, e13010.
Vance, M.E., Pegues, V., Van Montfrans, S., Leng, W., Marr, L.C., 2017. 'Aerosol emissions from fuse-deposition modeling 3D printers in a chamber and in real indoor environments'. Environ. Sci. Technol. 51, 9516–9523.
Viitanen, A.-K., Kallonen, K., Kukko, K., Kanerva, T., Saukko, E., Hussein, T., Hämeri, K., Säämänen, A., 2021. Technical control of nanoparticle emissions from desktop 3D printing. Indoor Air 31, 1061–1071.
Yi, J., LeBouf, R.F., Duling, M.G., Nurkiewicz, T., Chen, B.T., Schwegler-Berry, D., Virji, M.A., Stefaniak, A.B., 2016. 'Emission of particulate matter from a desktop three-dimensional (3D) printer'. J. Toxicol. Environ. Health, Part A 79, 453–465.
Zhang, Q., Wong, J.P.S., Davis, A.Y., Black, M.S., Weber, R.J., 2017. 'Characterization of particle emissions from consumer fused deposition modeling 3D printers'. Aerosol Sci. Technol. 51, 1275–1286.